Parameter Estimation and Line Width Control of Robot Guided Inkjet Deposition

Bashir Hosseini Jafari, Namhyung Lee, Bogdan Antohe and Nicholas Gans

Abstract— **In the field of inkjet deposition, there is a lack of specific knowledge to detect and change drop volume to regulate fluid placement. In this paper, we present a novel control scheme to regulate drop diameter on a surface with unknown properties. We derive a model for line width as a function of nozzle velocity, valve duty cycle, and physical properties of fluid and surface. As many of these variables are generally unknown, we present a nonlinear estimator to estimate their cumulative effects as a single variable. Next, benefiting from our estimation knowledge, a closed-loop control method is designed to track a time-varying line width. Stability of both the estimator and control are established using Lyapunov stability theory, and the control is shown to be robust to errors in the estimator. Simulations and experimental results confirm the stability and performance of the approach.**

I. Introduction

Inkjet deposition (or inkjet printing) refers to multiple technologies to deposit liquids on a substrate. Depositing of various liquid materials has been reported for many applications. Conductive ink has been used to print low-cost antennas on a paper substrate [1], [2]. Organic semiconductors have been printed to create transistors [3] and displays [4], [5]. Inkjet deposition has been used to deposit nerve regeneration conduits [6], biomaterials and tissues [7] [8]. Solutions of carbon nanotubes have been inkjet printed [9]. A mobile robot equipped with laser scanner and inkjet printer head was used to autonomously navigate a building and mark structures [10].

In this paper, we present preliminary results on inkjet deposition on arbitrary level surfaces. Researchers have used feedback control to improve deposition/ printing quality in other ways. Learning control was used to regulate jetting frequency and improve line quality [11]. Feed-forward and optimal control were used to reduce vibration in the reservoir and minimize variation in velocity and volume of drops [12], [13]. Control of the meniscus of the drop at the nozzle improved line uniformity [14]. Position [15] and velocity [16]–[18] control of the print head and substrate have been investigated.

Our work focuses on a novel control methodology and technology with an ultimate goal to print on a 3D surface of arbitrary shape. There are three major contributions in this paper. First we present a dynamic model of line width as a function of changing duty cycle, nozzle velocity and the contact angle arising from chemical and physical properties of the liquid and surface. Using the duty cycle as input and the width as output, we can obtain control-affine dynamics. However, many terms in the dynamic equations are unknown or difficult to measure. This leads to our second contribution, a nonlinear estimator to determine the cumulative uncertainties as a single parameter. The third contribution is a nonlinear control law to regulate drop diameter. The net result is a closed-loop regulation of printed line width given no knowledge of the interactions between liquid and surface. We also establish the robustness of this methods with respect to parameter error, which guarantees ultimate convergence of error to a known maximum value. The upper bound for the error depends on our control gain and difference between real and estimated parameter value. Stability of the estimator and control law is established through Lyapunov Analysis. Simulations and experiments are presented to verify performance of the estimation and control schemes.

The paper proceeds as follows. Section II presents derivations of spot volume with respect to duty cycle. Section III presents parameter estimation and section IV introduces a feedback controller to regulate spot diameter on a level surface. In section V and VI, we provide simulation and experimental results to verify the proposed method. Finally we present conclusion and future work in section VII.

II. Factors of Drop Volume and Line Width

We refer to a small amount of liquid in the air having recently left the jetting nozzle as a *drop*, while the liquid in contact with a surface is referred to as a *spot*. A spot deposited on a solid substrate will flatten and spread. The degree to which a drop of liquid spreads on a solid surface is referred to as *wetting* [19], [20]. Wetting is a complex phenomenon dependent on the chemical properties of the liquid, solid surface and surrounding air, physical properties of the solid such as surface roughness, temperature, and possible contamination such as dirt, oil, etc. Drop volume has the strongest influence on spot size, followed by fluid viscosity and surface interactions. Drop velocity and impact dynamics are generally negligible for small drops if the impact is normal to the surface. A second factor influencing line width is drop-to-drop spacing. Constant velocity of the nozzle mitigates changes in line width due to spacing. Single spot diameter determined by wetting defines the minimum line width, and reduction in spacing between drops/spots

This material is based upon work supported by the National Science Foundation under Grant No. 1563424,

B. Jafari, Namhyung Lee, and N. Gans are members of the Department of Electrical and Computer Engineering; B. Antohe is with Microfab Technologies Inc., Plano, TX {bxh140430, nxl160830, ngans}@utdallas.edu; bogdan.antohe@microfab.com .

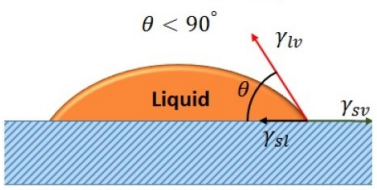

Fig. 1. Wetting and Contact Angle

increases the line width. Research has investigated proper spot spacing for different liquids and surfaces.

Wetting is typically studied in terms of contact angles, which describe the shape of the spot on a level surface. Small contact angles ($\theta < 90^o$) indicate high wetting and large spread, while large angles indicate low wetting and little spread. Young's equation [21] gives the contact angle θ at equilibrium as a function of the liquid-vapor, solid-vapor, and solid-liquid interfacial tensions (γ_{lv}, γ_{sv} and γ_{sl}) respectively, $\cos\theta = \frac{\gamma_{sv}-\gamma_{sl}}{\gamma_{lv}}$ (Fig. 1). The diameter of a drop/spot on the surface, as viewed from above, can be described as a function of the spot volume V and contact angle [22]. Depending on θ, the spot diameter d is

$$\begin{aligned} &\text{If } \theta < 90^o,\ d = 2(\frac{3}{\pi})^{1/3}\frac{\sin\theta}{(2+\cos\theta)^{1/3}(1-\cos\theta)^{2/3}}V^{1/3} \\ &\text{If } \theta > 90^o,\ d = 2(\frac{3}{\pi})^{1/3}\frac{1}{(2+\cos\theta)^{1/3}(1-\cos\theta)^{2/3}}V^{1/3}. \end{aligned} \tag{1}$$

Given accurate knowledge of the material properties, it is possible to estimate θ off-line and determine the correct volume for a drop to give a desired diameter. While research has gone into control to correctly generate the desired volume, if there is error in the estimate of θ, the diameter will be incorrect. Given a desired spot diameter d^*, define the error in spot diameter as $e(t) = d(t) - d^*(t)$. Consider the case of $\theta < 90^o$, and assume θ is constant. As the volume of liquid in a spot must be the same as volume in the drop before it contacts the surface, change of spot diameter is a function of the drop volume

$$\dot{d} = \frac{dd}{dV}\frac{dV}{dt} = \frac{\frac{2}{3}(\frac{3}{\pi})^{1/3}(\sin\theta)V^{-\frac{2}{3}}}{(2+\cos\theta)^{1/3}(1-cos\theta)^{2/3}}\dot{V}. \tag{2}$$

Collecting the constant terms as

$$b = \frac{\frac{2}{3}(\frac{3}{\pi})^{1/3}\sin\theta}{(2+\cos\theta)^{1/3}(1-cos\theta)^{2/3}} \tag{3}$$

the relationship between $\dot{d}$ and $\dot{V}$ can be written as

$$\dot{d} = bV^{-\frac{2}{3}}\dot{V}. \tag{4}$$

Equation (1) also can be represented

$$d = 3bV^{\frac{1}{3}} \tag{5}$$

or

$$V = (\frac{d}{3b})^3. \tag{6}$$

By substituting (6) in (4), we obtain

$$\dot{d} = 9\frac{b^3}{d^2}\dot{V}. \tag{7}$$

If the liquid is regulated by a solenoid valve, and the nozzle is moved at a constant velocity, then the volume of the drop is a function of the duty cycle of a signal sent to the valve. Let D denote the duty cycle of the signal. Within a specific range of duty cycle (e.g. $0 < D < 50$) the relationship between $\dot{V}$ and $\dot{D}$ is approximately linear

$$\dot{V}(t) = \alpha\dot{D}(t) \tag{8}$$

in which case $\dot{d}(t)$ can be written

$$\dot{d} = 9\frac{b^3}{d^2}\alpha\dot{D}(t) = \frac{B}{d^2}\dot{D}(t). \tag{9}$$

To give (9) a control affine form, we design $\dot{D}$ as

$$\dot{D} = ad^3 + d^2u \tag{10}$$

with u as our virtual input and a as our free parameter, giving the overall dynamics

$$\dot{d} = aBd + Bu. \tag{11}$$

B encapsulates all uncertainties and depends on surface and liquid characteristics. However, B is constant for a uniform surface and liquid and constant end-effector velocity (assuming that there is no dirt, oil, etc. on the surface).

III. Estimation of Constant Parameters Affecting Line Width

We consider our model as

$$\begin{aligned} \dot{d} &= aBd + Bu \\ y &= d \end{aligned} \tag{12}$$

and our estimator model

$$\begin{aligned} \dot{\hat{d}} &= a\hat{B}d + \hat{B}u \\ \hat{y} &= \hat{d} \end{aligned} \tag{13}$$

where $\hat{B}(t)$ is updated according to

$$\dot{\hat{B}} = k_1\hat{B} + k_2\hat{e} \quad k_1 < 0, k_2 > 0 \tag{14}$$

and $\hat{e} = d - \hat{d}$. Now, we are set to propose our theorem.

Theorem 1 Consider the system model in (12), and the estimator in (13), where $\hat{B}(t)$ is updated according to (14). If the control is given by $u = -ad+1$, then $e_B = B - \hat{B}(t)$ is bounded and converges to the zero as time goes to the infinity.

Proof First and second time derivative of e_B can be written as

$$\dot{e_B} = -\dot{\hat{B}} \tag{15}$$

and using (14),

$$\ddot{e}_B = -(k_1\dot{\hat{B}} + k_2\dot{\hat{e}}). \tag{16}$$

On the other hand, $\dot{\hat{e}} = \dot{d} - \dot{\hat{d}}$. Replacing (12) and (13) in $\dot{\hat{e}} = \dot{d} - \dot{\hat{d}}$, gives

$$\dot{\hat{e}} = (ad + u)e_B. \tag{17}$$

By replacing (15) and (17) in (16), we have

$$\ddot{e}_B = k_1 \dot{e_B} - k_2(ad + u)e_B \tag{18}$$

and designing $u = -ad + 1$ leads to the ordinary differential equation.

$$\ddot{e}_B - k_1 \dot{e_B} + k_2 e_B = 0. \tag{19}$$

Because roots of the characteristic equations of (19) are both negative, then e_B is bounded and converges to the zero as time goes to the infinity. This implies $\hat{B}$ is bouned and converges to B. We note that $\hat{B}$ is always positive, if its initial value is positive and $k_{1,2}$ render an over damped differential equation in (19).

IV. Diameter Control

After estimating B, we need to design a control scheme that guarantees the current diameter d converges to and tracks d^*.

A. Line Width Tracking Control

Theorem 2 Consider the system model in (12), and assuming that parameter B is known, then by designing

$$u = -ad + \frac{1}{B}(-k_3 e_t + \dot{d^*}) \quad k_3 > 0 \tag{20}$$

where $e_t = d - d^*$, one can guarantees d converges to d^* when time goes to infinity.

Proof Define our Lyapunov function as

$$V = \frac{1}{2} e_t^2. \tag{21}$$

Taking the time derivative of (21) and using (12) and (20), we arrive at

$$\begin{aligned} \dot{V} = e_t \dot{e_t} &= e_t(\dot{d} - \dot{d^*}) \\ &= e_t(aBd - aBd - k_3 e_t + \dot{d^*} - \dot{d^*}) \\ &= -k_3 e_t^2 \end{aligned} \tag{22}$$

which assures e_t goes to zero.

Where d^* is constant, (20) can be simplified to

$$u = -ad - \frac{k_3}{B}(e_t) \quad k_3 > 0 \tag{23}$$

B. Control Under Parameter Uncertainty

Due to sensor noise and errors, we likely have that e_B is small but not 0. Furthermore, there could be minor changes in B due to surface inconstancies. In these cases, the tracking control might not guarantee a perfect convergence. Here, we analyze the case that there are errors in our estimate of B, and show that we can guarantee e_t converges to a known neighborhood close to 0 and remains there. Furthermore, the size of this neighborhood can be determined through our choice of feedback gain. Knowing $\hat{B}$ is our estimate, the control in (20) would be

$$u = -ad + \frac{1}{\hat{B}}(-k_3 e_t + \dot{d^*}) \quad k_3 > 0 \tag{24}$$

and equation (22) can be rewritten as

$$\begin{aligned} \dot{V} = e_t \dot{e_t} &= e_t(\dot{d} - \dot{d^*}) \\ &= e_t(aBd - aBd + \frac{B}{\hat{B}}(-k_3 e_t + \dot{d^*}) - \dot{d^*}) \\ &= e_t(-k_3 \frac{B}{\hat{B}} e_t) + e_t \dot{d^*}(\frac{B}{\hat{B}} - 1) \\ &= -k_3 \frac{B}{\hat{B}}(e_t - \frac{(B - \hat{B})\dot{d^*}}{2k_3 B})^2 + \frac{(B - \hat{B})^2 {\dot{d^*}}^2}{4k_3 \hat{B} B} \end{aligned} \tag{25}$$

We can deduce that for $\hat{B}(t) > 0$, when

$$\left| e_t - \frac{\dot{d^*}(B - \hat{B})}{2k_3 B} \right| > \left| \frac{\dot{d^*}(B - \hat{B})}{2k_3 B} \right| \tag{26}$$

$\dot{V} < 0$ and guarantees asymptotically stability. However, for

$$\left| e_t - \frac{\dot{d^*}(B - \hat{B})}{2k_3 B} \right| \leq \left| \frac{\dot{d^*}(B - \hat{B})}{2k_3 B} \right| \tag{27}$$

$\dot{V}$ is not necessarily negative. As B and k_3 are constants, and $\hat{B}$ is bounded by some maximum, we can conclude that $\exists M \in \mathbb{R}_+$ such that $\left| \frac{\dot{d^*}(B - \hat{B})}{2k_3 B} \right| \leq M$. So, one can say the tracking error e_t will ultimately converge inside an interval with radius less than or equal to $2M$. That guarantees e_T is uniformly ultimately bounded. We also note that as $\hat{B} \to B$, $\left| \frac{\dot{d^*}(B - \hat{B})}{2k_3 B} \right| \to 0$.

V. Simulations

In this section, we test our estimator and control scheme under ideal conditions (e.g., there is no dirt or fluid/material characteristic change during the simulation) using Simulink. We set $B = 0.5$ and constant. The desired line diameter is a sinusoidal function as

$$d^* = 2\sin(t) + 2 \tag{28}$$

which varies between 0 and 4 mm. We first simulate estimation of B. Then, based on the estimation, we use the tracking controller to follow desired line diameter.

In Fig. 2, one can see that for different initial value of $\hat{B} = \{0.1, 0.3, 0.7, 1\}$, the estimate converges to the correct value of B, in less than 2 seconds, for $k_1 = -10$ and $k_2 = 25$. These values satisfy critical damping of the second order system (19).

In Fig. 3, one can see tracking performance of the control law in (20) using $B = 0.5$. We set $k_3 = 1$, $a = 1$. The blue graph is the desired line width, and the red graph is the measured width. The tracking error converges to zero in less than 3 seconds. In Fig. 4, the green graph depicts the duty cycle of the valve signal, which is calculated based on (10). Duty cycle is smooth and bounded from above and below.

In real experiments, B is not constant due to different factors like dirt, surface non-coherence, etc. In this part, we

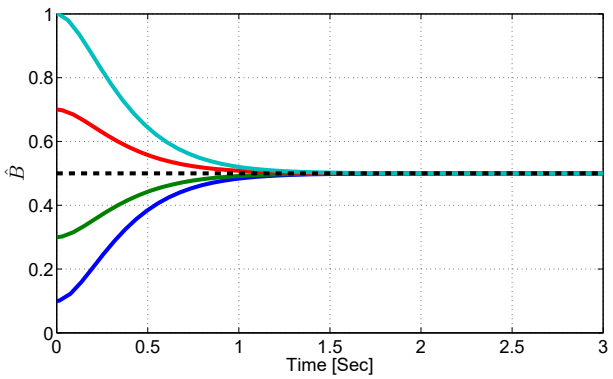

Fig. 2. Estimator Convergence for Different Initial Value

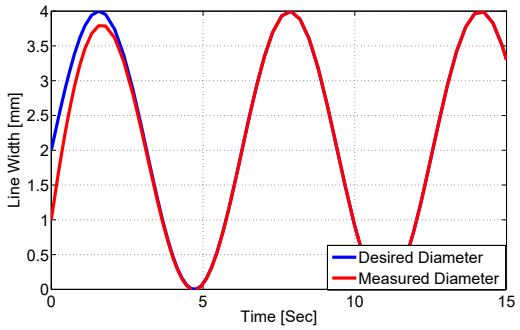

Fig. 3. Tracking Convergence without Parameter Uncertainty

simulate a situation in which B varies between 0.4 and 0.6 due to aforementioned factors. We used a random variable with mean of 0.5 and variance 0.1 with saturation limits of 0.4 and 0.6.

Using control law (24) with the worst case scenario of $\hat{B} = \{0.6, 0.4\}$, we expect an error interval

$$\begin{aligned} |e_t - (\pm 0.2)| &< 0.2 \\ -0.4 < e_t &< 0.4. \end{aligned} \tag{29}$$

Fig. 5 verifies our claim, as tracking error absolute value is bounded by ± 0.4. Fig. 6 depicts the duty cycle values corresponding to control under parameter uncertainty.

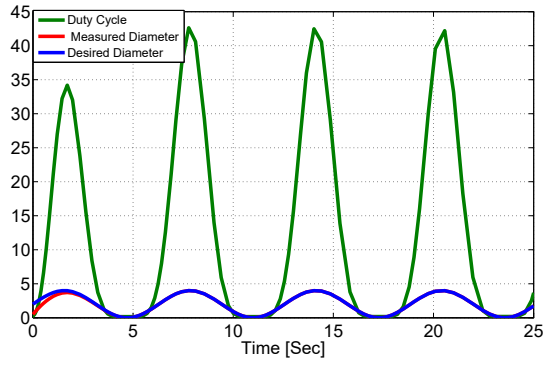

Fig. 4. Duty Cycle without Parameter Uncertainty

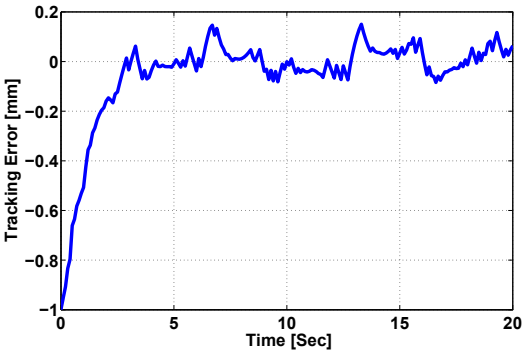

Fig. 5. Tracking Error with Parameter Uncertainty

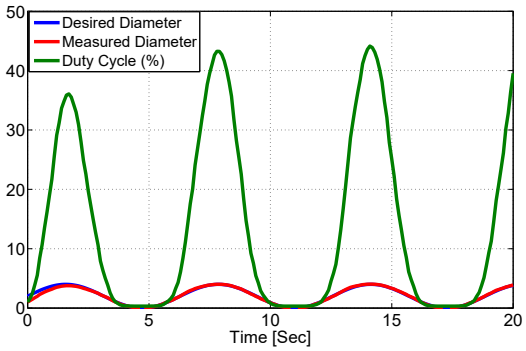

Fig. 6. Tracking Performance with Parameter Uncertainty

VI. Experiments

We conducted experiments to verify the estimation of B and control of line width proposed in Section III. As seen in Fig. 7, a Staubli TX90 robot arm has a solenoid valve mounted to the end effector. The needle mount was designed in Solidworks and machined such that the offset from the end effector flange is precisely known. We also mounted an Intel RealSense R300 RGB-D camera on the end effector. The camera can provide depth measurement to a sub-millimeter accuracy. The solenoid valve (INKX0514100A) is driven by a pulse train generated by an Arduino microcontroller, then

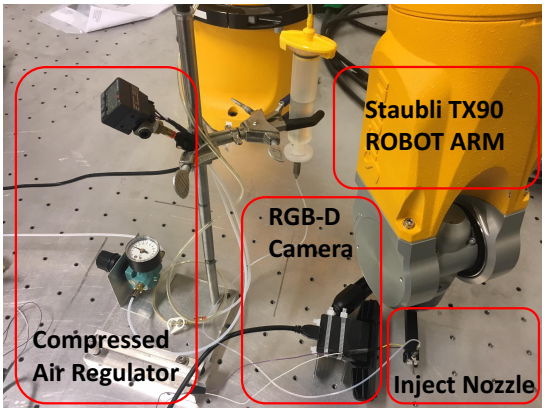

Fig. 7. Experiment Setup for Inkjet Printing

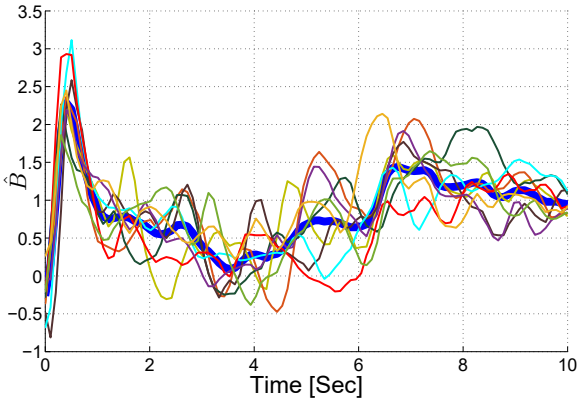

Fig. 8. B Estimation in 8 Different Experiments

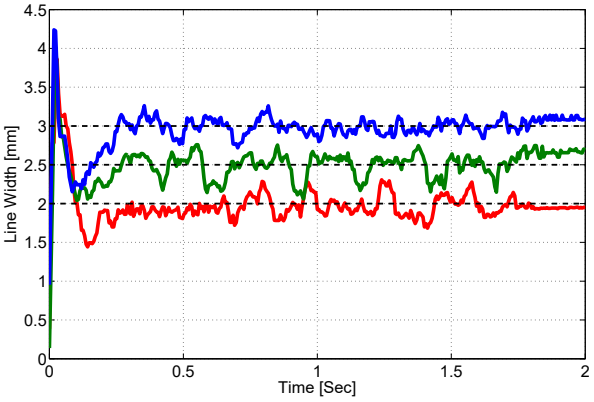

Fig. 10. Experiments of Regulation to Constant Line Width

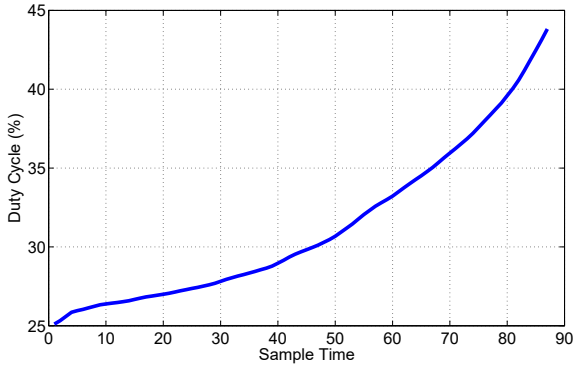

Fig. 9. Duty Cycle During B Estimation

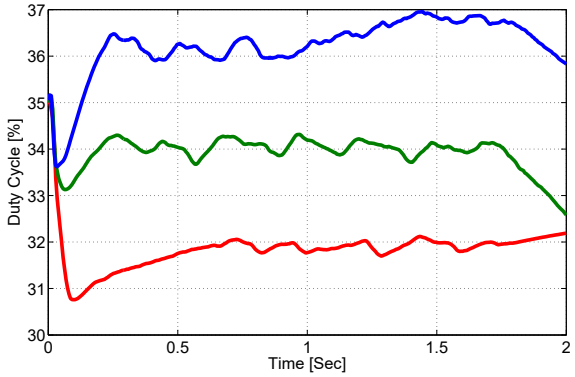

Fig. 11. Duty Cycle During Tracking

amplified to the necessary voltages levels. A compressed air tank with a digital regulator provides air pressure to a syringe filled with distilled water. To estimate line width, we converted the RGB image from the RealSense camera into a grayscale image, then isolated the ink mark below the needle by thresholding the grayscale image. An open morphological filter operation is applied to remove noise, such as water splatter marks in the image. We then find the biggest contour in our region of interest. Measuring the area and perimeter of that contour, leads us to line width in terms of number of pixels. By applying depth information, we measure line width in mm. Finally, a FIR filter was applied to reduce the measurement noise.

A. Estimation of B

We first provide results of estimation by applying the approach in Theorem 1. We set $k_1 = -10$, $k_2 = 25$ and $a = 1$. However, due to errors and uncertainties in real experiments, the estimate does not converge to a constant. Rather, oscillation around a constant value can be observed. We conducted eight different experiments, the results of which are shown as thin lines in Fig. 8. the mean of all experiments is also shown as a thick line. We observe that $\hat{B}$ converges to 1 approximately.

We also observed the duty cycle during estimation phase, as shown in Fig. 9. Note that there is no line width control involved in this part, and the line depth increases over time as duty cycle increases. In our experience, the estimate of $\hat{B}$ always converged before the duty cycle saturated. Choice of gains $k1$ and $k2$, as well as the magnitude of the control $u(t)$ could mitigate saturation if it becomes an issue.

B. Regulation to Constant Desired Line Width

Fig. 10 depicts three experiments to regulate line width to constants values of 3.0mm, 2.5mm, and 2.0mm. We set $k_3 = 1$, and the duty cycle initial value was $D = 35$. One can see that the measured line width converges near desired value with some oscillation. The corresponding duty cycles are shown in Fig. 11. Photos of the lines are shown in Fig. 12 and photos of line width measurements are provided in Fig. 13. The calipers are in inches, but we can note that the measurements are approximately 0.079"=2mm, 0.098"=2.49mm and 0.118"=3.0mm, indicating that our approach works well.

C. Tracking a Time Varying Desired Value

Two experiments for time varying line width are shown, with the desired width given by sine functions $d^* = \sin(2t) + 3$ and $d^* = \sin(0.5t) + 3$. The initial value of the duty cycle was set to 35. Figs. 14 and 16 show line width observed during experiment, and Figs. 15, and 17 depict the corresponding duty cycle. The line width quickly converges

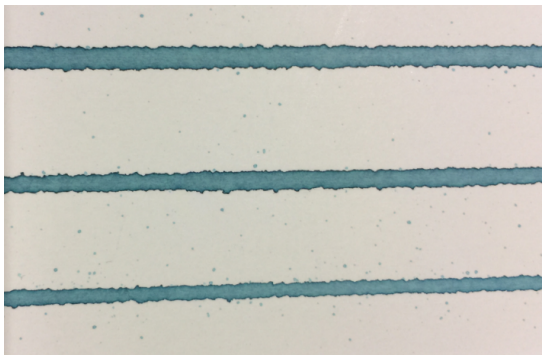

Fig. 12. Printed lines width, from top to bottom the desired widths are 3.0, 2.5, and 2.0mm

Fig. 13. Line width Measurements in inches

near the desired value and tracks well after that, though noise is evident in the measured signal. Printed lines are shown in Fig. 18. Maximum and minimum widths of the lines are also measured in Fig. 19 which are approximately 4 mm and 2 mm respectively, as expected.

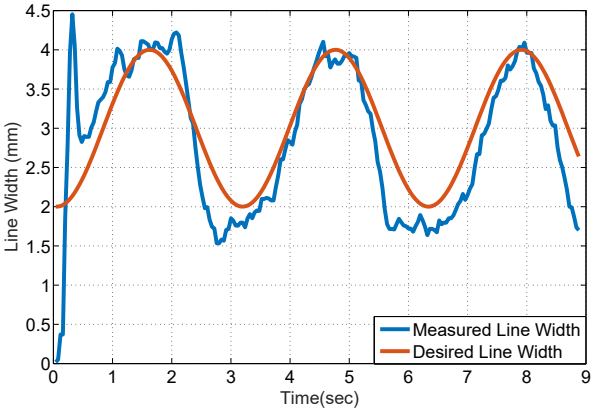

Fig. 14. Tracking Performance with Sinusoidal Line Width

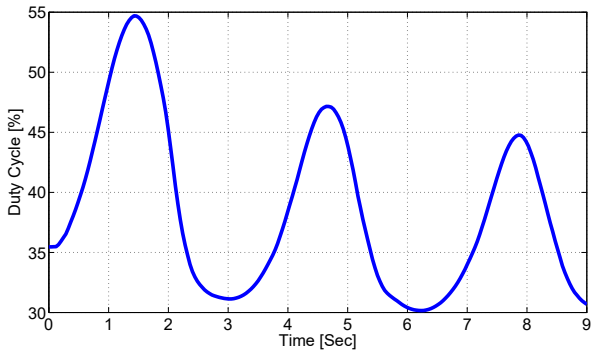

Fig. 15. Duty Cycle During Tracking

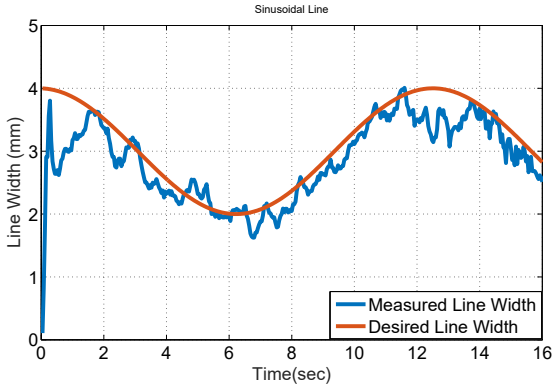

Fig. 16. Tracking Performance with Sinusoidal Line Width

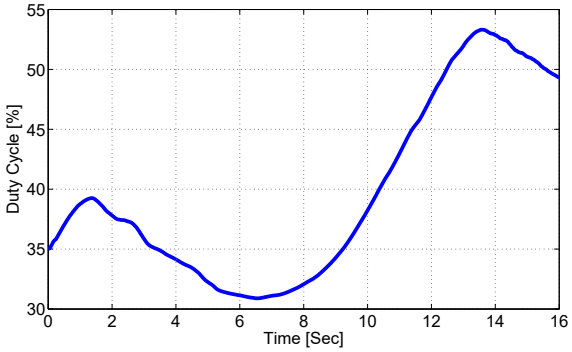

Fig. 17. Duty Cycle During Tracking

VII. Conclusions and Future Work

This paper described an investigation into how to model, estimate and control an inkjet device mounted on a robot end effector to draw a line with a desired width in a closed loop fashion. This nonlinear estimation allows us to estimate parameters of the model with no knowledge about physical properties of the surface and fluid. We established the robustness of our method to parameter estimation error and the stability of our closed loop system. Simulations and experiments validated the performance of the approach for constant and time varying desired widths.

Our ultimate goal is to deposit ink with a desired width on

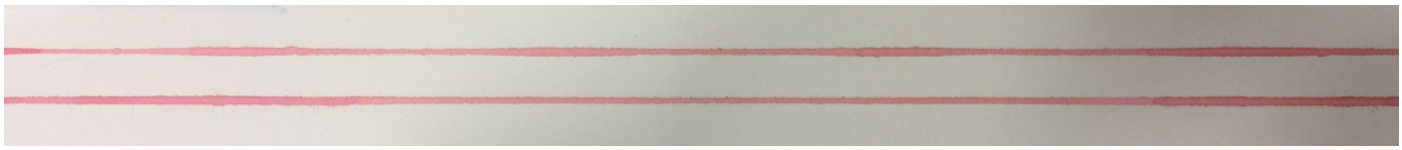

Fig. 18. Printed lines with $\omega = 2$ (top) and $\omega = 0.5$ (bottom)

Fig. 19. Line width measurement in inch

a given path on a 3D surface. Motion planning of the robot end effector is our next step to be investigated. Equation (8) is also a simplification of the real system dynamic, so we are interested in deriving a much detailed differential equation that describe valve deposition dynamics. We are currently investigating an approach to a combined nonlinear estimator and controller, rather than the two phase process presented here. One remaining technical issue is that our camera is not reliable for sub millimeter measurements. This lack of precise knowledge causes experiments to deviate from the ideal result observed in simulation.

REFERENCES

[1] V. Lakafosis, A. Rida, R. Vyas, L. Yang, S. Nikolaou, and M. Tentzeris, "Progress towards the first wireless sensor networks consisting of inkjet-printed, paper-based rfid-enabled sensor tags," *Proceedings of the IEEE*, vol. 98, no. 9, pp. 1601–1609, 2010.

[2] G. Shaker, S. Safavi-Naeini, N. Sangary, and M. Tentzeris, "Inkjet printing of ultrawideband (uwb) antennas on paper-based substrates," *IEEE Antennas and Wireless Propagation Letters*, vol. 10, pp. 111–114, 2011.

[3] M. Shtein, P. Peumans, J. Benziger, and S. Forrest, "Direct, mask- and solvent-free printing of molecular organic semiconductors," *Advanced Materials*, vol. 16, no. 18, pp. 1615–1620, 2004.

[4] S.-C. Chang, J. Liu, J. Bharathan, Y. Yang, J. Onohara, and J. Kido, "Multicolor organic light-emitting diodes processed by hybrid inkjet printing," *Advanced Materials*, vol. 11, no. 9, pp. 734–737, 1999.

[5] S. R. Forrest, "The path to ubiquitous and low-cost organic electronic appliances on plastic," *Nature*, vol. 428, no. 6986, pp. 911–918, 2004.

[6] D. Silva, D. Wallace, P. Cooley, D. Radulescu, and D. Hayes, "An inkjet printing station for neuroregenerative tissue engineering," in *IEEE Engineering in Medicine and Biology Workshop*, pp. 71–73, 2007.

[7] B. Lorber, W.-K. Hsiao, I. M. Hutchings, and K. R. Martin, "Adult rat retinal ganglion cells and glia can be printed by piezoelectric inkjet printing," *Biofabrication*, vol. 6, no. 1, p. 015001, 2014.

[8] T. Burg, R. Groff, K. Burg, M. Hill, and T. Boland, "Systems engineering challenges in inkjet biofabrication," in *SoutheastCon, 2007. Proceedings. IEEE*, pp. 395–398, 2007.

[9] K. Kordás, T. Mustonen, G. Tóth, H. Jantunen, M. Lajunen, C. Soldano, S. Talapatra, S. Kar, R. Vajtai, and P. M. Ajayan, "Inkjet printing of electrically conductive patterns of carbon nanotubes," *Small*, vol. 2, no. 8-9, pp. 1021–1025, 2006.

[10] P. Jensfelt, E. Forell, and P. Ljunggren, "Field and service applications - automating the marking process for exhibitions and fairs - the making of harry platter," *IEEE Robotics Automation Magazine*, vol. 14, no. 3, pp. 35–42, 2007.

[11] S. Mishra, K. Barton, and A. Alleyne, "Control of high-resolution electrohydrodynamic jet printing," in *American Control Conference*, pp. 6537–6542, 2010.

[12] M. Ezzeldin, P. van den Bosch, and S. Weiland, "Toward better printing quality for a drop-on-demand ink-jet printer: improving performance by minimizing variations in drop properties," *IEEE Control Systems*, vol. 33, no. 1, pp. 42–60, 2013.

[13] A. Khalate, X. Bombois, G. Scorletti, R. Babuska, S. Koekebakker, and W. de Zeeuw, "A waveform design method for a piezo inkjet printhead based on robust feedforward control," *Journal of Microelectromechanical Systems*, vol. 21, no. 6, pp. 1365–1374, 2012.

[14] T. K. Nguyen, V. D. Nguyen, D. Byun, and J. ParkN, "Stabilizing meniscus shape to improve pattern uniformity in drop-on-demand ehd inkjet printing using visual feedback," in *International Conference on Control, Automation and Systems*, pp. 392–394, 2012.

[15] Z. Ye, Y. He, R. Pieters, B. Mesman, H. Corporaal, and P. Jonker, "Demo: An embedded vision system for high frame rate visual servoing," in *ACM/IEEE International Conference on Distributed Smart Cameras*, pp. 1–2, 2011.

[16] J. van Helvoort, B. de Jager, and M. Steinbuch, "Data-driven controller unfalsification with analytic update applied to a motion system," *IEEE Transactions on Control Systems Technology*, vol. 16, no. 6, pp. 1207–1217, 2008.

[17] H. Y. Lin, M. C. Lu, J. H. Horng, T. B. Yang, S. C. Hsieh, C. Y. Hsiao, H. M. Tai, and J. Chen, "Dc servo speed control of an inkjet print head transport system using a phase-locked loop," in *Proceedings International Workshop on Advanced Motion Control*, vol. 2, pp. 458–463 vol.2, 1996.

[18] C. Chen, C. Cheng, and G.-C. Chiu, "Adaptive robust control of media advance systems for thermal inkjet printers," *Mechatronics*, vol. 10, no. 12, pp. 111 – 126, 2000.

[19] D. Myers, *Wetting and Spreading*, pp. 415–447. John Wiley & Sons, Inc., 2002.

[20] D. Bonn, J. Eggers, J. Indekeu, J. Meunier, and E. Rolley, "Wetting and spreading," *Rev. Mod. Phys.*, vol. 81, pp. 739–805, May 2009.

[21] T. Young, "An essay on the cohesion of fluids," *Philosophical transactions*, 1805.

[22] D. Quéré, M.-J. Azzopardi, and L. Delattre, "Drops at rest on a tilted plane," *Langmuir*, vol. 14, no. 8, pp. 2213–2216, 1998.